Int. J. Heat Mass Transfer. Vol. 27, No. 10, pp. 1749–1757, 1984
Printed in Great Britain

0017–9310/84 $3.00 + 0.00

Penetrative convection in porous medium bounded by a horizontal wall with hot and cold spots

DIMOS POULIKAKOS
Department of Mechanical Engineering, P.O. Box 4348,
University of Illinois at Chicago, Chicago, IL 60680, U.S.A.

and

ADRIAN BEJAN
Department of Mechanical Engineering, Campus Box 427, University of Colorado,
Boulder, CO 80309, U.S.A.

(*Received* 2 *August* 1983 *and in revised form* 12 *December* 1983)

Abstract—This paper reports a series of numerical simulations and a scale analysis of the penetrative convection occurring along the unevenly heated horizontal wall of a semi-infinite porous medium. Modeling the problem as two-dimensional, and assuming that the horizontal wall temperature varies between alternating hot and cold spots, it is found that the natural circulation consists of a row of counter-rotating cells situated near the wall. Each cell penetrates vertically into the porous medium to a distance approximately equal to $\lambda Ra_\lambda^{1/2}$, where λ is the distance between a hot spot and the adjacent cold spot, and Ra_λ is the Darcy-modified Rayleigh number based on λ and on the temperature difference between each spot and the porous medium situated far enough from the wall. The ability of each cell to convect heat between two adjacent spots increases with the Rayleigh number. The results of numerical simulations in the Ra_λ range 1–100 are found to support a number of scaling laws derived based on pure scaling arguments.

INTRODUCTION

IN THIS paper we focus on an interesting occurrence of natural convection in a semi-infinite fluid-saturated porous medium, namely, the cellular flow that grows in the vicinity of a horizontal boundary whose temperature varies periodically. The system geometry is presented schematically in Fig. 1, and a representative sample of the ensuing flow pattern is shown in Figs. 2–4. This natural convection phenomenon is interesting for a number of reasons. First, it belongs to a relatively unknown class of buoyancy-driven flows termed 'penetrative convection', that is, flows covering only a small part of the medium into which they are driven. The overwhelming majority of the natural convection studies found in the literature has been dedicated to 'enclosed' flows, i.e. to flows which fill the entire porous medium. Recent reviews of natural convection in porous media demonstrate that the enclosed flows are becoming a classical subfield, one where earlier developments have been confirmed by a relatively large number of subsequent studies [1, 2].

Penetrative flows, on the other hand, seem to have escaped scrutiny despite their common occurrence in nature. We are aware of only two studies of penetrative convection in porous media, the vertical penetration into a well filled with porous medium, with application to the grain storage problem [3], and the lateral penetration into a horizontal porous structure, with application to the natural-convection cooling of rotating electric windings [4]. Both studies have shown that the shape of these flows and the volume filled by them depends on appropriately defined Rayleigh numbers (i.e. on the local temperature differences that drive them).

The present study addresses an entirely new type of penetrative convection problem, in that it focuses on a semi-infinite isothermal porous medium heated and cooled from below periodically. This configuration is most relevant to understanding the behavior of underground porous layers heated unevenly. It will be based on computer simulations and on scale analysis shown, that two adjacent spots (one hot, the other cold) on the horizontal boundary drive a natural convection cell vertically into the porous medium. It will also be shown how the height of vertical penetration of each cell and the cells' ability to transfer heat between the two spots, increase with the spot-to-spot temperature difference. The main features of this penetrative convection phenomenon will be summarized in the form of scaling laws validated by numerical simulations.

MATHEMATICAL FORMULATION

The two-dimensional model shown in Fig. 1 represents an infinite impermeable horizontal plate adjacent to a semi-infinite fluid saturated porous material. It is assumed that the temperature of the plate is a periodic function of the horizontal coordinate $\hat{x}$. Two simple functions for plate temperature will be

NOMENCLATURE

c_p fluid specific heat at constant pressure
f function of Rayleigh number, equation (32)
g gravitational acceleration
H height of the rectangular domain chosen for numerical simulations
h vertical penetration height, Fig. 5
k thermal conductivity of (fluid/porous matrix) composite
K permeability
Nu Nusselt number, equation (18)
P pressure
Q net heat transfer rate, equation (19) [W m^{-1}]
Ra_λ Rayleigh number based on λ, equation (16)
T temperature
ΔT maximum spot temperature relative to the temperature infinitely far from the wall, equations (1) and (2)
u horizontal velocity component
v vertical velocity component
x horizontal Cartesian coordinate
y vertical Cartesian coordinate.

Greek symbols
α thermal diffusivity of porous medium, $k/\rho c_p$
β coefficient of thermal expansion
δ thickness of the flow section parallel to the wall, Fig. 5
θ temperature scale of region 3, Fig. 5
λ half-period of the wall temperature variation, Fig. 1
μ viscosity
ν kinematic viscosity, μ/ρ
ρ fluid density
ψ streamfunction.

Subscripts
∞ pertaining to the region sufficiently far from the vicinity of the horizontal wall
f pertaining to the fluid.

Symbols
$\hat{}$ dimensional quantity.

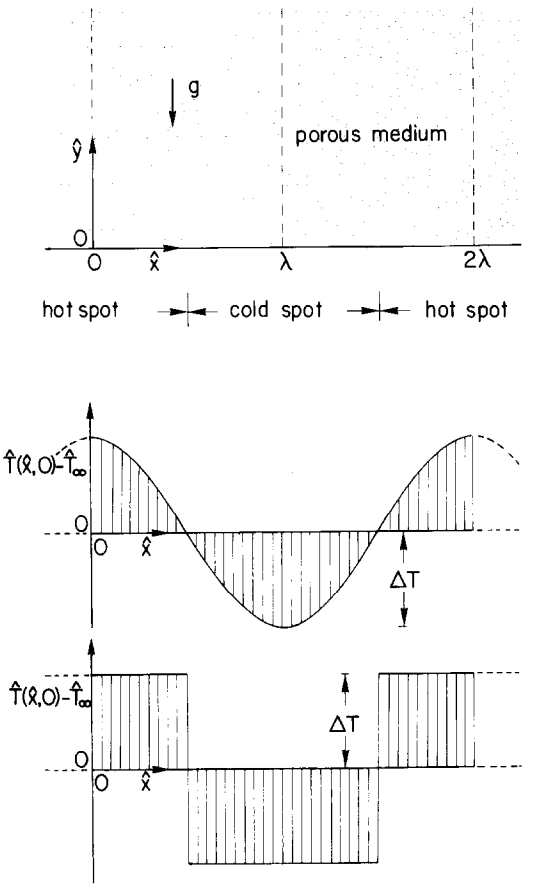

FIG. 1. Semi-infinite porous medium bounded by an impermeable horizontal wall with periodic heating and cooling.

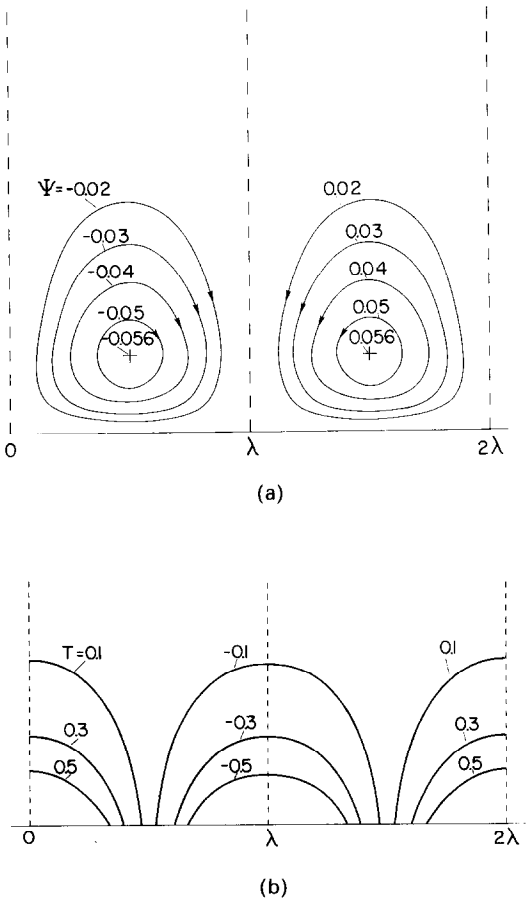

FIG. 2. Patterns of streamlines and isotherms for $Ra_\lambda = 1$ and cosine wall temperature variation.

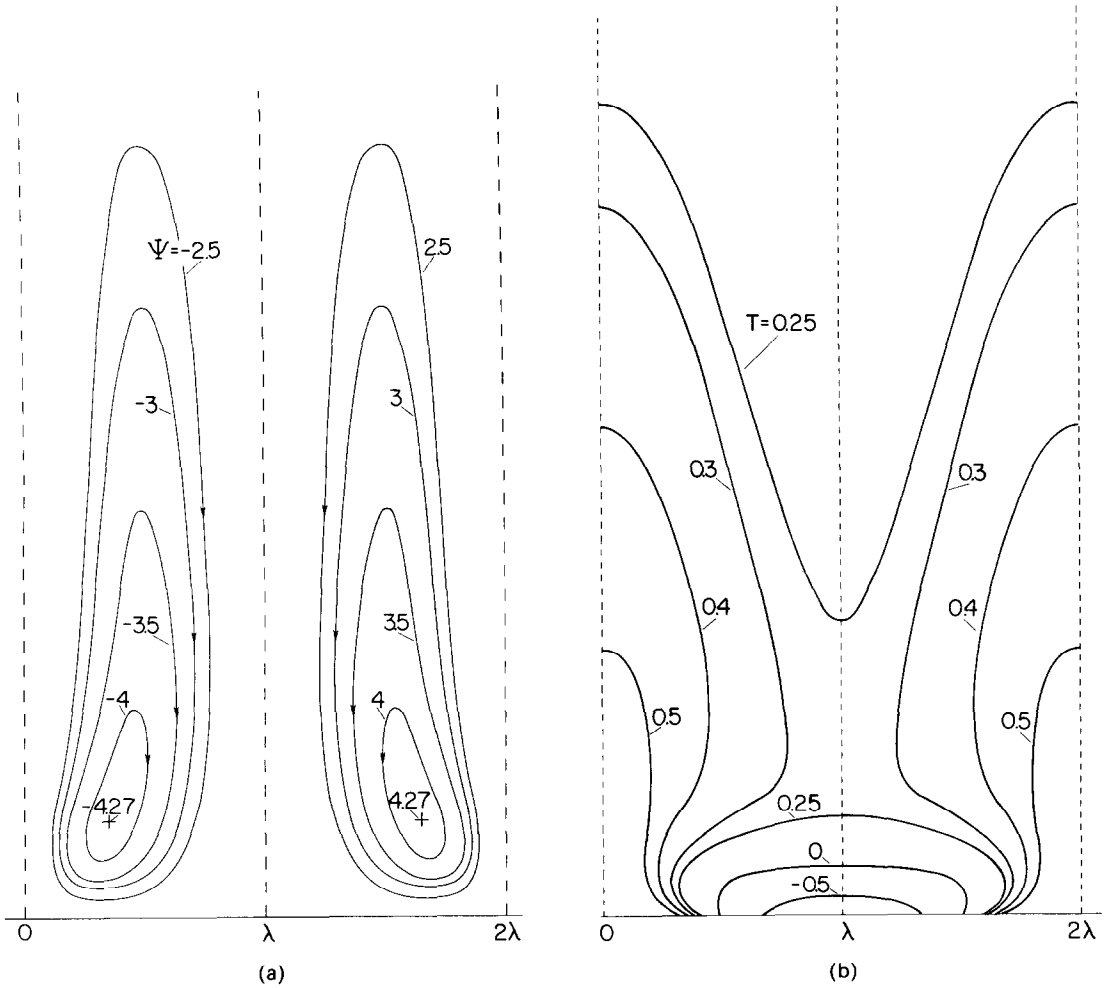

FIG. 3. Patterns of streamlines and isotherms for $Ra_\lambda = 100$ and cosine wall temperature variation.

considered, the cosine variation

$$\hat{T}(\hat{x},0)-\hat{T}_\infty = \Delta\hat{T}\cos\frac{\pi\hat{x}}{\lambda} \tag{1}$$

and the step function

$$\hat{T}(\hat{x},0)-\hat{T}_\infty = \begin{cases} \Delta\hat{T}, & 0 \leqslant \hat{x} < \dfrac{\lambda}{2} \\ -\Delta\hat{T}, & \dfrac{\lambda}{2} < \hat{x} < \dfrac{3\lambda}{2} \\ \Delta\hat{T}, & \dfrac{3\lambda}{2} < \hat{x} \leqslant 2\lambda. \end{cases} \tag{2}$$

In the above equations 2λ is the period (i.e. the shortest distance between two hot spots) and $\Delta\hat{T}$ is the amplitude of the plate temperature variation. Subscript '∞' stands for 'sufficiently far away from the vicinity of the horizontal surface' and $\hat{T}_\infty$ is assumed to be constant.

In accordance with the homogeneous porous medium model [1], the equations governing the steady-state conservation of mass, momentum and energy in the porous space of Fig. 1 are

$$\frac{\partial\hat{u}}{\partial\hat{x}}+\frac{\partial\hat{v}}{\partial\hat{y}}=0 \tag{3}$$

$$\hat{u} = -\frac{K}{\mu}\frac{\partial\hat{P}}{\partial\hat{x}} \tag{4}$$

$$\hat{v} = -\frac{K}{\mu}\left(\frac{\partial\hat{P}}{\partial\hat{y}}+\rho g\right) \tag{5}$$

$$\hat{u}\frac{\partial\hat{T}}{\partial\hat{x}}+\hat{v}\frac{\partial\hat{T}}{\partial\hat{y}} = \alpha\left(\frac{\partial^2}{\partial\hat{x}^2}+\frac{\partial^2}{\partial\hat{y}^2}\right)\hat{T}, \tag{6}$$

where $\hat{u}, \hat{v}, \hat{\mu}, \hat{P}$ and $\hat{T}$ are the fluid velocity components, the viscosity, the pressure and the temperature. The two momentum equations are based on the Darcy flow model whereby K represents the permeability of the porous matrix. The effective thermal diffusivity of the medium is defined as $\alpha = k/(\rho c_p)_f$, where k is the thermal conductivity of the porous material filled with motionless fluid. It is assumed that the fluid is locally in thermal equilibrium with the solid porous matrix.

Modeling the flow as 'Boussinesq-incompressible' to take into account the coupling between the energy and

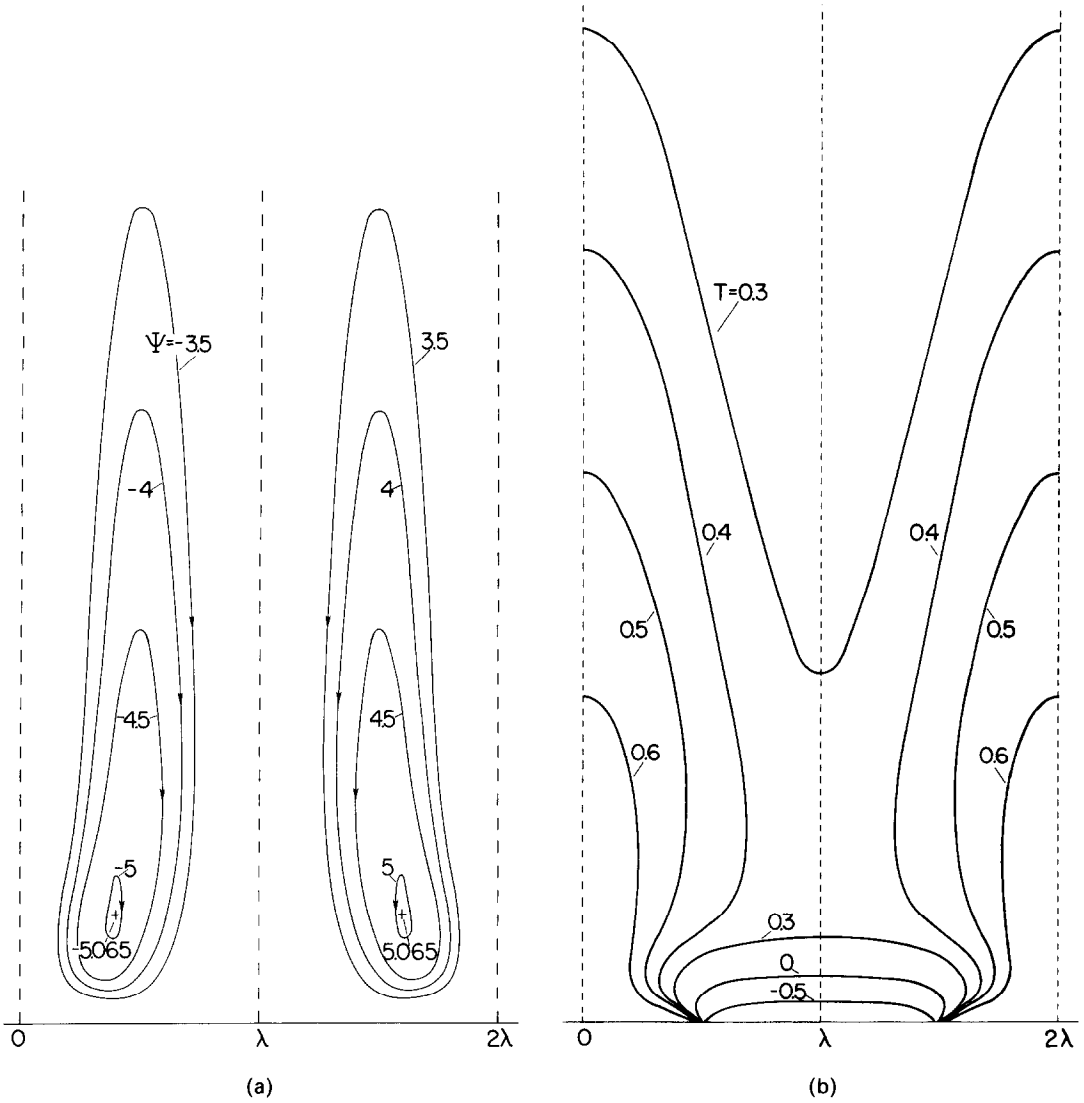

FIG. 4. Patterns of streamlines and isotherms for $Ra_\lambda = 100$ and step-function wall temperature variation.

momentum equations, we regard the density ρ as constant everywhere except in the body force term of equation (5) where it is replaced by

$$\rho \cong \rho_0[1-\beta(T-T_0)]. \tag{7}$$

In this equation the subscript '0' refers to a reference state, and β is the coefficient of thermal expansion of the fluid. Eliminating the pressure terms between equations (4) and (5) and introducing the streamfunction

$$\hat{u} = \frac{\partial \hat{\psi}}{\partial \hat{y}}, \quad \hat{v} = -\frac{\partial \hat{\psi}}{\partial \hat{x}} \tag{8, 9}$$

yields a unique momentum conservation statement

$$\left(\frac{\partial^2}{\partial \hat{x}^2} + \frac{\partial^2}{\partial \hat{y}^2}\right)\hat{\psi} = -\frac{Kg\beta}{\nu}\frac{\partial \hat{T}}{\partial \hat{x}}. \tag{10}$$

Relative to the system sketched in Fig. 1, the task is to solve the system of equations (6) and (8)–(10) subject to the following boundary conditions

$$\begin{aligned}
&\hat{v} = 0, \quad \hat{T} \text{ described by equation (1) or (2) at } \hat{y} = 0\\
&\hat{u} = 0, \quad \text{at } \hat{x} = 0 \quad \text{(symmetry)}\\
&\hat{u} = 0, \quad \text{at } \hat{x} = \lambda \quad \text{(symmetry)}\\
&\hat{u} = 0, \quad \text{at } \hat{x} = 2\lambda \quad \text{(symmetry)}\\
&\hat{v} = 0, \quad \hat{T} \to \hat{T}_\infty \quad \text{as } \hat{y} \to \infty.
\end{aligned} \tag{11}$$

In what follows we rely on both numerical and scale analyses to determine the chief properties of the vertical penetration phenomenon driven by the nonuniform temperature of the horizontal boundary.

NUMERICAL SOLUTION

If we define $\Delta\hat{T}$, λ, α and α/λ as reference unit dimensions for temperature variation, length, streamfunction and velocity, respectively, we can introduce

the following dimensionless variables

$$x = \hat{x}/\lambda, \quad y = \hat{y}/\lambda, \quad \psi = \hat{\psi}/\alpha, \quad T = \frac{\hat{T}-\hat{T}_\infty}{\Delta\hat{T}}$$
$$u = \hat{u}/(\alpha/\lambda), \quad v = \hat{v}/(\alpha/\lambda). \tag{12}$$

The governing equations and boundary conditions corresponding to this dimensionless notation are

$$\nabla^2\psi = -Ra_\lambda \frac{\partial T}{\partial x} \tag{13}$$

$$\frac{\partial(uT)}{\partial x} + \frac{\partial(vT)}{\partial y} = \nabla^2 T \tag{14}$$

$v = 0, \quad \psi = 0$ and T determined from equations (1) and (2); at $y = 0$

$$u = 0, \quad \psi = 0 \quad \text{at } x = 0, 1, 2$$
$$v = 0, \quad \psi = 0 \quad \text{and } T = 0 \quad \text{at } y = H/\lambda \tag{15}$$

where $H/\lambda \gg 1$ is the aspect ratio of the rectangular domain chosen for numerical simulations. In equation (13), Ra_λ is the Darcy-modified Rayleigh number based on the half-period of the plate temperature variation, λ

$$Ra_\lambda = \frac{Kg\beta\lambda\Delta T}{\nu\alpha}. \tag{16}$$

Due to the symmetry of the boundary conditions sketched in Fig. 1, only the left half of the problem needs to be solved ($0 \leqslant x \leqslant 1$, Fig. 1). The numerical solution for the right half ($1 \leqslant x \leqslant 2$) is simply the mirror image of the solution for the left half.

The numerical solution of equation (14) was determined using an unconditionally stable finite-difference scheme proposed by Allen and Southwell [5]. This scheme was later tested successfully against a number of other finite-difference schemes, by Chow and Tien [6]. The Allen–Southwell method is an exponential method and its detailed formulation is omitted here for it can be found in refs. [5, 6]. The streamfunction field was obtained from equation (13) using the successive overrelaxation method [7, 8] and a known temperature distribution.

The region of interest was covered with m vertical and n horizontal grid lines. We used a uniform grid with $m = 41$ vertical grid lines, even though $m = 21$ yielded reasonable results also. The number of horizontal grid lines (i.e. the domain height H) necessary to obtain an accurate solution depends on the height of flow penetration into the unbounded porous matrix, hence, it depends on both Ra_λ and the temperature distribution along the horizontal surfaces. In each case, in order to determine the appropriate value of n we sought the minimum number of horizontal grid lines that yielded a solution satisfying the far-field boundary conditions ($\psi = 0$, $T = 0$) within prescribed error. As shown in Table 1, the largest number of horizontal grid lines necessary for an accurate solution was $n = 287$ for the case of $Ra_\lambda = 100$ and step-function plate temperature, equation (2). As an additional check, in all cases we calculated $\partial T/\partial y$ at $y = H/\lambda$ and found it to be practically zero. Therefore, despite the finiteness of the domain used for numerical analysis, the fluid situated far from the wall was not affected by the hot and cold spots maintained along the horizontal wall.

The final numerical solutions for flow and temperature resulted from an iterative process which was repeated until the following criterion was satisfied

$$\frac{\sum_{i=1}^{m}\sum_{j=1}^{n} |\phi_{i,j}^{r+1} - \phi_{i,j}^{r}|}{\sum_{i=1}^{m}\sum_{j=1}^{n} |\phi_{i,j}^{r+1}|} < 10^{-4}. \tag{17}$$

In this criterion ϕ refers to T and ψ, while r denotes the iterative cycle.

The net heat transfer rate Q from the warm region $0 \leqslant x \leqslant 1/2$ to the cold region $1/2 \leqslant x \leqslant 1$ was determined numerically and cast in Nusselt-number form

$$Nu = \frac{Q}{k\Delta\hat{T}}. \tag{18}$$

The net heat transfer rate is defined as

$$Q = -\int_0^{\lambda/2} k\left(\frac{\partial\hat{T}}{\partial\hat{y}}\right)_{\hat{y}=0} d\hat{x}. \tag{19}$$

In terms of the dimensionless quantities defined in equation (12) the Nusselt number is

$$Nu = -\int_0^{1/2} \left(\frac{\partial T}{\partial y}\right)_{y=0} dx. \tag{20}$$

Equation (20) was integrated numerically after the final temperature field was obtained. A relation similar to equation (20) is obtained by integrating the heat flux along the cold wall region $1/2 \leqslant x \leqslant 1$. This second Nusselt number calculation was carried out, and the results were found to be nearly identical to the values yielded by equation (20); the discrepancy between the two Nusselt numbers was less than 2% throughout this study.

Representative patterns of streamlines and isotherms are shown in Figs. 2–4. The special cases selected for graphic illustration are intended to show two effects,

Table 1. Numerical results for heat and fluid flow in a semi-infinite porous medium bounded by an impermeable horizontal wall with alternating hot and cold spots*

Ra_λ	Nu	ψ_{max}	H/λ (or n/m)
1	1.006 (2.242)	0.0557 (0.0749)	4
10	1.024 (2.3)	0.5805 (0.7679)	4
20	1.124 (2.503)	1.135 (1.457)	5
40	1.387 (2.961)	2.083 (2.54)	5
60	1.636 (3.36)	2.87 (3.454)	6
80	1.85 (3.7)	3.6 (4.274)	7
100	2.05 (3.99)	4.27 (5.065)	7

* The numbers in parentheses correspond to the step-function distribution of wall temperature, equation (2), and the others to the cosine distribution, equation (1).

namely, the effect of Rayleigh number and the effect of wall temperature variation. Moving from Fig. 2 to Fig. 3, we see that the Rayleigh number governs the vertical distance to which the natural convection cells penetrate into the porous medium. The 'penetration height' increases visibly as the Rayleigh number Ra_λ increases. Furthermore, as shown by the Nu and ψ_{max} values in Table 1, the net spot-to-spot heat transfer rate and the mass flow rate of each cell increase monotonically as the Rayleigh number increases.

Next, comparing Fig. 3 with Fig. 4 we find that the choice of wall temperature function, equations (1) and (2), has a relatively weak impact on the vertical penetration pattern. In the case of step-function variation of wall temperature, Fig. 4, the cells appear to be narrower as they position themselves above the temperature steps (which are located at $\hat{x} = \lambda/2$ and $3\lambda/2$).

When, as in Fig. 3, the wall temperature varies smoothly from ΔT to $-\Delta T$, each natural convection cell is spread more evenly over the wall section of length λ situated between points of maximum and minimum temperature. The weak effect of wall temperature function is illustrated further by the cell flow rates (ψ_{max}) reported in Table 1. However, the heat transfer rate (Nu) is noticeably larger in the case of step-function wall temperature, suggesting the presence of intense local heat flux in the immediate vicinity of the temperature steps.

The heat and fluid flow trends discovered numerically and documented in Figs. 2–4 and Table 1 can be predicted analytically on the basis of pure scaling arguments. To explain these trends is the objective of the next section. However, before focusing attention on scale analysis, it is useful to keep in mind that the flow and temperature patterns reported in Figs. 2–4 show only the lower extremity of the slender domain (of height H and horizontal width λ) in which the problem was solved numerically. In all cases, the rectangular domain of each numerical solution was considerably taller than the region illustrated in the figures.

SCALE ANALYSIS

Consider the main components of the penetrative flow (Fig. 5):

(1) the section parallel to the wall;
(2) the vertical hot plume;
(3) the vertical downflow driven back into the wall section 1.

The flow extends vertically to a height h: this penetration height is one of the objectives of scale analysis. The thickness of the section parallel to the wall is also unknown and labelled δ. The variation of fluid temperature around the loop 1–2–3–1 sketched in Fig. 5 requires special attention. Although the temperature variation along the wall length λ is of the order of $2\Delta T$, the fluid loop temperature variation is not as pronounced. To see this, follow the rise of hot plume

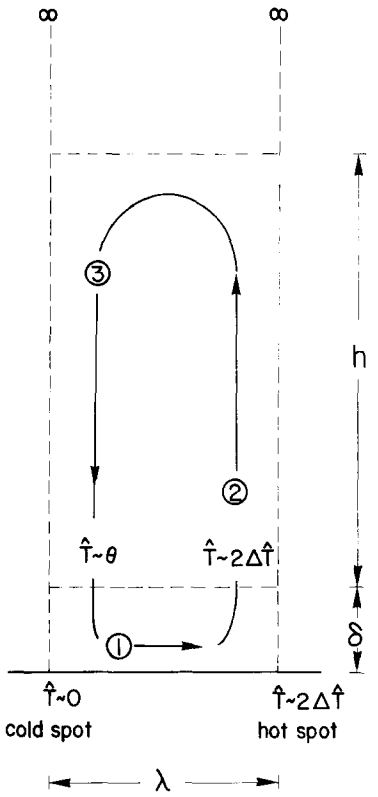

FIG. 5. Definition of flow regions and temperature scales used in scale analysis.

fluid through region 2: the temperature of this fluid is of the order of $2\Delta\hat{T}$, as this stream has just detached from the wall. Eventually, this hot stream must turn around to fill the vacuum created in the beginning of region 1. The hot stream returns through region 3, and it hits region 1 at a temperature higher than the cold spot temperature $\hat{T} \sim 0$. Let the temperature scale of region 3 be $\hat{T} \sim \theta$. The temperature scale θ must be greater than zero, because only then will the cold spot be able to recapture the energy poured into the cellular flow by the hot spot. In conclusion, the cellular flow experiences temperatures between a high order $2\Delta T$ and a low order θ.

The scaling laws required by the governing equations are as follows. For region 1 near the impermeable wall, the momentum equation (10) states that

$$\left(\frac{\hat{u}}{\delta} \text{ or } \frac{\hat{v}}{\lambda}\right) \sim \frac{Kg\beta}{\nu}\frac{2\Delta\hat{T}-\theta}{\lambda}, \tag{21}$$

where the velocity scales $(\hat{u}, \hat{v})$ are related through the mass continuity equation (3)

$$\frac{\hat{u}}{\lambda} \sim \frac{\hat{v}}{\delta}. \tag{22}$$

In order to decide which term to retain on the LHS of equation (21), we make the *assumption* that the wall region 1 is such that the δ scale is less than or, at most, equal to the λ scale (graphically, this assumption means that region 1 is either a boundary layer or, in the

extreme, a square). It is easy to see that if $\delta \leqslant \lambda$, then $\hat{u}/\delta \geqslant \hat{v}/\lambda$, therefore the momentum equation (21) implies

$$\hat{u} \sim \frac{Kg\beta}{\nu}(2\Delta\hat{T}-\theta)\frac{\delta}{\lambda}. \tag{23}$$

The flow rate through region 1 is

$$\hat{\psi} \sim \hat{u}\delta \sim \frac{Kg\beta}{\nu}(2\Delta\hat{T}-\theta)\frac{\delta^2}{\lambda}. \tag{24}$$

The vertical counterflow between regions 2 and 3 is driven by the horizontal temperature gradient between the two branches, $\partial\hat{T}/\partial x \sim (2\Delta T-\theta)/\lambda$. Assuming that regions 2 and 3 are vertically slender, $h \gg \lambda$, the momentum equation (10) requires

$$\frac{\hat{v}}{\lambda} \sim \frac{Kg\beta}{\nu}\frac{2\Delta\hat{T}-\theta}{\lambda}. \tag{25}$$

This also means that the flow rate through regions 2 and 3 is of the order of

$$\hat{\psi} \sim \hat{v}\lambda \sim \frac{Kg\beta}{\nu}(2\Delta\hat{T}-\theta)\lambda. \tag{26}$$

Comparing this estimate with the $\hat{\psi}$ scale obtained from region 1, equation (24), we conclude that the flow rate is conserved through each cell only if

$$\delta \sim \lambda, \quad \text{constant}. \tag{27}$$

Note that this conclusion is consistent with the $\delta \leqslant \lambda$ assumption that preceded equation (23). The same conclusion is supported by the streamline patterns of Figs. 2–4, where the 'cross' of maximum dimensionless stream-function $\hat{\psi}$ can be regarded as landmark for $\hat{y} \sim \delta$.

The vertical penetration height h follows from energy conservation arguments; looking again at the vertical counterflow between regions 2 and 3, and assuming once more that these regions are slender, the energy equation (6) requires

$$\hat{v}\frac{2\Delta\hat{T}-\theta}{h} \sim \alpha\frac{2\Delta\hat{T}-\theta}{\lambda^2}. \tag{28}$$

Combining equations (28) and (25), we find

$$\frac{h}{\lambda} \sim \frac{Kg\beta\lambda(2\Delta\hat{T}-\theta)}{\alpha\nu} \tag{29}$$

in other words, the slenderness ratio h/λ is the same as the Darcy-modified Rayleigh number based on λ and on the unknown temperature variation experienced by the fluid of one cell.

To determine the fluid temperature variation scale $(2\Delta\hat{T}-\theta)$, we must account for the continuity (conservation) of heat transfer between the cellular flow and the differentially heated spots on the wall. Relative to region 1 near the wall, the energy equation (6) implies the following equivalence of scales

$$\hat{u}\frac{2\Delta\hat{T}-\theta}{\lambda} \sim \alpha\frac{\theta}{\delta^2}. \tag{30}$$

Using the earlier conclusion that δ is of the order of λ, equation (27), and substituting the $\hat{u}$ scale given by equation (23), the energy balance (30) yields a relationship between θ and $\Delta\hat{T}$

$$Ra_\lambda \sim \frac{\theta/\Delta\hat{T}}{(2-\theta/\Delta\hat{T})^2} \tag{31}$$

where Ra_λ is the Darcy-modified Rayleigh number based on λ and ΔT, equation (16). The ratio $\theta/\Delta\hat{T}$ can be extracted explicitly from equation (31)

$$\frac{\theta}{\Delta\hat{T}} \sim f(Ra_\lambda) = 2+\frac{1}{2Ra_\lambda}-\left(\frac{2}{Ra_\lambda}+\frac{1}{4Ra_\lambda^2}\right)^{1/2}. \tag{32}$$

As shown in Fig. 6, θ approaches $2\Delta\hat{T}$ as Ra_λ increases, which means that the cell fluid becomes more isothermal around the 1–2–3–1 loop as the flow penetrates deeper into the semi-infinite medium, thus losing thermal contact with the cold spot on the boundary.

It is worth noting that the same relationship between θ and $\Delta\hat{T}$ could be derived from an integral scaling argument regarding the flow of energy from the hot spot to the cold spot via the cellular flow. The vertical counterflow of regions 2 and 3 carries enthalpy pumped into it by the hot spot at a rate of type $\dot{m}c_p\Delta\hat{T}$ of the order of

$$Q_{\text{in}} \sim \rho c_p \hat{v}\lambda(2\Delta\hat{T}-\theta) \tag{33}$$

where $\hat{v}$ is the vertical velocity scale in regions 2 and 3, equation (25). The cold spot captures this heat current via diffusion across a layer of thickness δ

$$Q_{\text{out}} \sim k\lambda\frac{\theta}{\delta}. \tag{34}$$

Setting $Q_{\text{in}} \sim Q_{\text{out}}$ yields the $\theta/\Delta\hat{T} \sim f(Ra_\lambda)$ relationship discovered previously, equation (31).

The penetration height scale h can now be expressed solely in terms of λ and Ra_λ, by combining equations (29) and (32)

$$\frac{h}{\lambda} \sim [2-f(Ra_\lambda)]\,Ra_\lambda. \tag{35}$$

This result is plotted on Fig. 6 alongside the other conclusions furnished by the scale analysis. It is evident that the slenderness ratio h/λ increases roughly as $Ra_\lambda^{1/2}$, demonstrating that the preceding analysis (which was based on the assumption that $h/\lambda \gg 1$) is valid in the high Rayleigh number limit, i.e. in the range $Ra_\lambda^{1/2} \gg 1$. Although the cases studied numerically comply only marginally with this 'high Ra_λ' requirement, the geometry of the penetrative flow shown in Figs. 2–4 agrees quantitatively with the order-of-magnitude predictions of scale analysis (Fig. 6). Further evidence that the slenderness ratio h/λ reaches $O(10)$ at $Ra_\lambda = 100$ is provided by the numerical solution: as shown in Table 1, the smallest slenderness ratio H/λ that proved adequate for numerical simulations at $Ra_\lambda = 100$ was 7.

Finally, the high Rayleigh number scale analysis

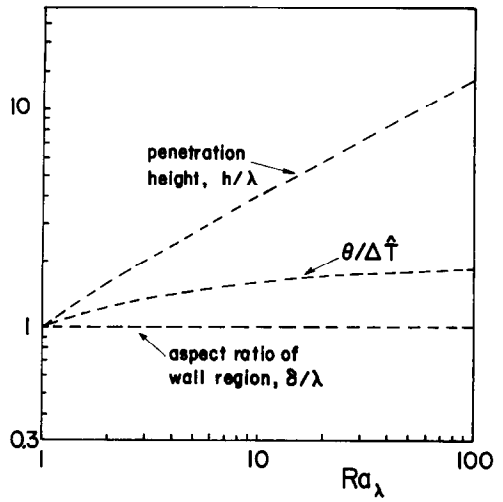

FIG. 6. Graphic summary of the results furnished by scale analysis.

developed above can serve to extrapolate towards the $Ra_\lambda \to \infty$ limit the flow and heat transfer results obtained numerically for moderate Rayleigh numbers, $1 < Ra_\lambda < 100$ (Table 1). The scale analysis suggests that in the high Ra_λ limit the cell flow rate must scale as

$$\hat{\psi} \sim \alpha Ra_\lambda [2 - f(Ra_\lambda)] \tag{36}$$

in other words

$$\frac{\hat{\psi}}{\alpha(2-f)Ra_\lambda} \sim O(1). \tag{37}$$

This scaling law is supported very strongly by the trend in the numerical data of Table 1 plotted on Fig. 7.

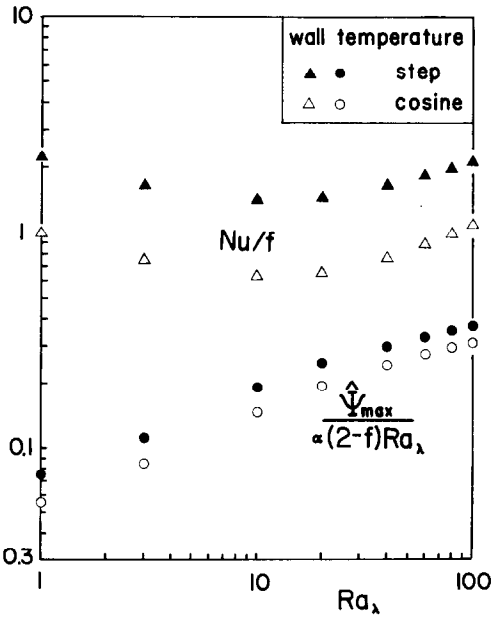

FIG. 7. Correlation of heat transfer rate and flow rate results according to predictions based on scale analysis.

The heat transfer rate in the $Ra_\lambda \to \infty$ limit is given by equations (32) and (33); in Nusselt number form, these expressions read

$$Nu = \frac{Q_{out}}{k\Delta\hat{T}} \sim \frac{\theta}{\Delta\hat{T}} \sim f(Ra_\lambda) \tag{38}$$

or

$$\frac{Nu}{f(Ra_\lambda)} \sim O(1). \tag{39}$$

Figure 7 shows that this scaling law is obeyed by all the numerical Nu data assembled in Table 1.

CONCLUSIONS

We found that a semi-infinite porous medium heated and cooled periodically from below (or from above) develops a cellular flow along the horizontal boundary (Figs. 2–4). Each cell is a deformed plume, in the sense that the hot plume rising above a hot spot is eventually turned around and sucked into the vacuum created around the closest cold spot (Fig. 5). As the Rayleigh number Ra_λ increases, the cellular natural circulation formed along the boundary contains fluid whose temperature resembles more closely the temperature of the hot spot, and not that of the porous medium situated infinitely far from the horizontal boundary. This temperature asymmetry of the cellular flow is due to the fact that the fluid in contact with the hot spot rises, thus fueling the flow, whereas the fluid in contact with the cold spot is trapped near the wall. If the periodically heated wall bounds the semi-infinite porous medium from above (not from below, as in Fig. 1), then the cellular flow formed along such a boundary contains fluid whose temperature resembles that of the cold spots.

Numerical simulations and scale analysis showed that the cellular flow penetrates the porous medium vertically to a distance approximately equal to $\lambda Ra_\lambda^{1/2}$, where λ is the distance between adjacent cold and hot spots (Fig. 6). The wall region of each cell, i.e. the turn-around region in which the deformed plume sinks and rises again, does not become a 'boundary layer' as Ra_λ increases: the thickness of this wall region continues to be of the same order of magnitude as its length λ (Figs. 2–6). The heat transfer rate between two adjacent spots increases monotonically as the Rayleigh number Ra_λ increases (Table 1). Throughout this study we showed order-of-magnitude agreement between heat and fluid flow features revealed by numerical simulations, and analytical predictions based on pure scaling arguments.

Acknowledgement—This research was conducted under the auspices of National Science Foundation Grant No. MEA-82-07779.

REFERENCES

1. P. Cheng, Heat transfer in geothermal systems, *Adv. Heat Transfer* **14**, 1–105 (1979).

2. A. Bejan, A synthesis of analytical results for natural convection heat transfer across rectangular enclosures, *Int. J. Heat Mass Transfer* **23**, 723–726 (1980).
3. A. Bejan, Natural convection in a vertical cylindrical well filled with porous medium, *Int. J. Heat Mass Transfer* **23**, 726–729 (1980).
4. A. Bejan, Lateral intrusion of natural convection into a horizontal porous structure, *Trans. Am. Soc. Mech. Engrs*, Series C, *J. Heat Transfer* **103**, 237–241 (1981).
5. D. N. de G. Allen and R. V. Southwell, Relaxation methods applied to determine the motion, in two dimensions, of a viscous fluid past a fixed cylinder, *Q. Jl Mech. Appl. Math.* **8**, 129–145 (1955).
6. L. C. Chow and C. L. Tien, An examination of four differencing schemes for some elliptic-type convection equations, *Num. Heat Transfer* **1**, 87–100 (1978).
7. P. J. Roache, *Computational Fluid Dynamics*, pp. 117–119. Hermosa, Albuquerque (1976).
8. C. Y. Chow, *An Introduction to Computational Fluid Mechanics*, pp. 160–161. Wiley, New York (1979).

CONVECTION PENETRANTE DANS UN MILIEU POREUX LIMITE PAR UNE SURFACE PLANE AVEC DES SPOTS CHAUDS ET FROIDS

Résumé—On rapporte une série de simulations numériques et une analyse de la convection pénétrante qui se produit à la paroi horizontale chauffée d'un milieu poreux semi-infini. La modélisation du problème est bidimensionnelle et elle suppose que la température de la surface varie entre des spots alternativement chauds et froids. On trouve que la circulation naturelle consiste en un réseau de cellules contrarotatives situé près de la surface. Chaque cellule pénètre verticalement dans le milieu poreux à une distance approximativement égale à $\lambda\, Ra^{1/2}$, où λ est la distance entre un spot chaud et le λ froid adjacent, et Ra_λ est le nombre de Rayleigh modifié selon Darcy, basé sur λ et sur la différence de température entre chaque spot et le milieu poreux situé loin de la surface. L'aptitude de chaque cellule à convecter entre deux spots adjacents agumente avec le nombre de Rayleigh. Les résultats des simulations numériques pour le domaine de Ra 1–100 autorisent un certain nombre de lois dérivées d'arguments basés sur la similitude.

EINDRINGENDE KONVEKTION IN EINEM PORÖSEN MEDIUM, DAS VON EINER HORIZONTALEN WAND MIT HEISSEN UND KALTEN STELLEN BEGRENZT IST

Zusammenfassung—Diese Abhandlung stellt eine Reihe numerischer Simulationsrechnungen und eine Modellbetrachtung bei eindringender Konvektion vor, die an einer ungleichmäßig beheizten, horizontalen Wand eines halbunendlichen porösen Mediums auftritt. Bei Annahme eines zweidimensionalen Problems und einer zwischen den abwechselnd heißen und kalten Stellen veränderlichen Wandtemperatur ergab sich, daß die freie Zirkulation aus einer Reihe entgegengesetzt drehender, wandnaher Zellen besteht. Jede Zelle dringt bis zu einer Entfernung von etwa $\lambda\, Ra_\lambda^{1/2}$ senkrecht in das poröse Medium ein, wobei λ der Abstand zwischen der heißen und der benachbarten kalten Stelle und Ra_λ die Darcy-modifizierte Rayleighzahl ist, die von λ und von der Temperaturdifferenz zwischen den einzelnen Stellen und dem porösen Medium in ausreichender Entfernung von der Wand abhängt. Die Fähigkeit jeder Zelle konvektiv Wärme zwischen zwei angrenzenden Stellen zu transportieren steigt mit der Rayleighzahl. Die Ergebnisse der numerischen Simulationsrechnungen im Bereich $1 \leqslant Ra_\lambda \leqslant 100$ ermöglichen die Ableitung einer Reihe von Modellgesetzen, denen reine Maßstabsparameter zugrunde liegen.

КОНВЕКЦИЯ В ПОРИСТОЙ СРЕДЕ, ОГРАНИЧЕННОЙ ГОРИЗОНТАЛЬНОЙ СТЕНКОЙ С НАГРЕТЫМИ И ХОЛОДНЫМИ УЧАСТКАМИ

Аннотация—Представлен ряд численных моделей и проведен анализ подобия для конвекции вдоль неравномерно нагреваемой горизонтальной стенки, ограничивающей полубесконечную пористую среду. Для двумерной модели при условии, что температура горизонтальной стенки непрерывно изменяется между нагретыми и холодными участками, найдено, что течение состоит из ряда вращающихся в противоположных направлениях ячеек, локализованных у стенки. Каждая ячейка проникает в пористую среду на расстояние, примерно равное $\lambda\, Ra_\lambda^{1/2}$, где λ—расстояние между соседними горячим и холодным участками, а Ra_λ—Дарси-модификация числа Рэлея, которое основано на λ и местной разности температур между каждым участком и пористой средой на достаточно большом расстоянии от стенки. Способность каждой ячейки переносить тепло между двумя соседними участками возрастает с увеличением числа Рэлея. В результате численного моделирования в интервале значений числа Ra_λ от 1 до 100 подтвержден ряд зависимостей, полученных на основе анализа подобия.